Published in final edited form as:
Bone. 2009 January ; 44(1): 17–23. doi:10.1016/j.bone.2008.08.126.

Myostatin (GDF-8) Deficiency Increases Fracture Callus Size, Sox-5 Expression, and Callus Bone Volume

Ethan Kellum[1], **Harlan Starr**[3], **Phonepasong Arounleut**[3], **David Immel**[4], **Sadanand Fulzele**[2,3], **Karl Wenger**[2,3], and **Mark W. Hamrick**[1,2,3,*]

1 *Department of Orthopaedic Surgery, Medical College of Georgia Augusta, GA USA*

2 *Institute of Molecular Medicine and Genetics, Medical College of Georgia Augusta, GA USA*

3 *Department of Cellular Biology and Anatomy, Medical College of Georgia Augusta, GA USA*

4 *Savannah River National Laboratory Aiken, SC USA*

Abstract

Myostatin (GDF-8) is a negative regulator of skeletal muscle growth and mice lacking myostatin show increased muscle mass. We have previously shown that myostatin deficiency increases bone strength and biomineralization throughout the skeleton, and others have demonstrated that myostatin is expressed during the earliest phase of fracture repair. In order to determine the role of myostatin in fracture callus morphogenesis, we studied fracture healing in mice lacking myostatin. Adult wild-type mice (+/+), mice heterozygous for the myostatin mutation (+/−), and mice homozygous for the disrupted myostatin sequence (−/−) were included for study at two- and four-weeks following osteotomy of the fibula. Expression of Sox-5 and BMP-2 were significantly upregulated in the fracture callus of myostatin-deficent (−/−) mice compared to wild-type (+/+) mice at two-weeks following osteotomy. Fracture callus size was significantly increased in mice lacking myostatin at both two- and four-weeks following osteotomy, and total osseous tissue area and callus strength in three-point bending were significantly greater in myostatin −/− mice compared to myostatin +/+ mice at four weeks post-osteotomy. Our data suggest that myostatin functions to regulate fracture callus size by inhibiting the recruitment and proliferation of progenitor cells in the fracture blastema. Myostatin deficiency increases blastema size during the early inflammatory phase of fracture repair, ultimately producing an ossified callus having greater bone volume and greater callus strength. While myostatin is most well known for its effects on muscle development, it is also clear that myostatin plays a significant, direct role in bone formation and regeneration.

Keywords

ActRIIB; BMP-2; Activin; Chondrogenesis; Osteogenesis

*Corresponding Author: Mark W. Hamrick, PhD, Department of Cellular Biology & Anatomy, Laney Walker Blvd. Augusta, GA 30912 USA, mhamrick@mail.mcg.edu, ph: 706-721-1958, fax: 706-721-6120.

Introduction

Myostatin, a member of the transforming growth factor-β superfamily of secreted growth and differentiation factors, is a negative regulator of skeletal muscle growth [1]. Myostatin null mice have approximately twice the skeletal muscle mass of normal mice, and naturally occurring mutations in the myostatin gene significantly increase muscle mass and decrease subcutaneous fat in a variety of animals, including humans [2]. Myostatin expression in skeletal muscle increases with weightlessness and unloading, and exogenous administration of myostatin causes muscle wasting [3]. Furthermore, loss or inhibition of myostatin function improves muscle regeneration following injury [4]. Utilizing in vitro and in vivo systems we have found that myostatin deficiency increases bone strength and biomineralization throughout the skeleton, including the limbs, spine, and jaw [5–7]. We have also identified the receptor for myostatin, the type IIB activin receptor (ActRIIB), in bone-marrow derived mesenchymal stem cells (BMSCs), and shown that BMSCs from myostatin-deficient animals have increased osteogenic potential [8]. These results suggest that myostatin may also play a role in regulating bone formation, which is further indicated by the recent discovery that a myostatin decoy receptor (ActRIIB-Fc) significantly increases bone formation and bone mass in mice [9]. In addition, it has been demonstrated that myostatin is highly expressed in the fracture callus immediately after injury [10], further revealing a direct role for this factor in bone development and morphogenesis.

Based on the findings referenced above, we propose that loss or inhibition of myostatin signaling may not only improve muscle regeneration following injury but may also alter bone and cartilage development following fracture. Here we test this hypothesis using a fibular osteotomy model in normal and myostatin-deficient mice. There are several well-established protocols for inducing bone fractures in rodents, including cutting the tibia at the midshaft, which requires inserting a pin internally to stabilize the fracture, and fracturing the femur by applying blunt force to the thigh, which also requires internal fixation. A fibular osteotomy model was chosen because, in mice, the fibula serves as a non-weight-bearing bone that does not require internal fixation after osteotomy [11]. We studied the effects of myostatin deficiency on fracture callus size, cartilage and bone volume in the fracture callus, and the expression of osteogenic (col1, BMP-2, Osx, and Runx-2) and chondrogenic (Sox5, Sox9) genes in the callus with the expectation that these parameters would be significantly altered in mice lacking myostatin.

Materials and Methods

Animals

Male and female myostatin-deficient mice ($Mstn^{-/-}$), mice heterozygous for the myostatin mutation ($Mstn^{-/+}$), and wild type mice ($Mstn^{+/+}$) on a CD-1 background, 6–8 months of age, were used to evaluate the effects of myostatin deficiency on fracture healing. Development of the fracture callus was assessed radiographically and histologically in 8–10 mice per genotype at two weeks post-osteotomy and in 8–10 mice per genotype at four weeks post-osteotomy. Mice were raised in the animal care facility at the Medical College of Georgia and are derived from the breeding colony described previously [8,12]. All mice were housed in the same room and given food and water ad libitum. This study was approved by the Institutional Animal Care and Use Committee of the Medical College of Georgia.

Surgical procedure and tissue preparation

Mice were placed under isoflurane anesthesia, and anesthesia was verified using toe pinch. The hair from the lateral side of the left hind leg was shaved, and the leg cleaned with betadine and ethyl alcohol. A 5–7 mm incision was made along the lateral side of the leg approximately

12 mm proximal to the calcaneal tuberosity. For the fibular osteotomy, the midshaft of the fibula was exposed by blunt dissection and a transverse fracture was made in the fibula with microtenotomy scissors. The surgical wound was closed using skin glue (3M Vetbond, Saint Paul MN). The animal was removed from the nose cone and given a subcutaneous injection of ketoralac (15mg/kg) immediately following the surgical procedure and 24 hours after surgery. Mice were euthanized by CO_2 overdose and thoracotomy two weeks and four weeks following surgery. After euthanizing the mouse, the left hind limb was skinned, the quadriceps muscle dissected free, removed and weighed. The leg was then disarticulated at the knee and ankle and fixed in cold paraformaldehyde for 24 hours. Specimens were washed and transferred to 70 percent alcohol.

Radiographic Imaging

The limbs were radiographed using a Faxitron small-animal x-ray cabinet at 35kVP, 2.5 mA for 15 seconds. Callus diameter was measured from Faxitron radiographs using Sigma Scan image analysis software and normalized by diameter of the fibular shaft for calculation of a fracture callus index. Representative specimens were sent to the Savannah River Site National Laboratory (Aiken, SC) for micro-computed tomography using a 160 kV micro-focus X-ray machine (Kevex Inc., Model 16010), a four-axis positioning system (New England Affiliated Technologies series 300), and an amorphous silicon imager (Varian Inc, Paxscan 4030).

Histology and Histomorphometry

Specimens were decalcified in 4% EDTA, washed, dehydrated, embedded in paraffin and sectioned transversely at 8 μm using a rotary microtome. Sections of the fracture callus were stained with safranin-O and fast green to assess total callus area, cartilage area and bone area, and using celestine-blue-van Gieson stain for illustrations of callus size. Section images were captured using a Leica compound DMLS microscope with digital camera attachment and computer interface. Total callus area (C.Ar), total osseous tissue area (TOT.Ar), and cartilage area (Cg.Ar) were measured using SigmaScan image analysis software. Histomorphometric nomenclature follows standards recommended by Gerstenfeld et al. [13].

Real-time PCR

The majority of specimens were used for the histological analysis described above, however fractured fibulas from an additional six wild-type ($Mstn^{+/+}$) and six myostatin-deficient ($Mstn^{-/-}$) mice were also used for preparation of mRNA two-weeks following the osteotomy procedure. The callus was carefully isolated after removal of muscles and callus tissue homogenized in Trizol. The samples were assayed for absorbance at 260 nm (Helios-Gamma, Thermo Spectronic, Rochester, NY), then reverse transcribed using iScript reagents from Bio-Rad on a programmable thermal cycler (PCR-Sprint, Thermo Electron, Milford, MA). 50 ng complementary deoxyribonucleic acid (cDNA) was amplified in each 40-cycle real-time polymerase chain reaction using a Bio-Rad iCycler, ABgene reagents (distributed by Fisher) and custom designed primers and probes specific to the mouse genome (Table 1). Data were analyzed as described previously [8].

Biomechanical Testing

Fractured fibulas from five wild-type ($Mstn^{+/+}$) and five myostatin-deficient ($Mstn^{-/-}$) mice were used for biomechanical testing four-weeks following the osteotomy procedure. The proximal ligamentous junction between the tibia and fibula was carefully separated with a scalpel, and a wire saw was used to separate the fused tibia and fibula distally. Specimens were tested in three-point bending using a Vitrodyne V1000 Materials Testing system. Fibulas were mounted on stainless steel fixtures 5 mm apart, approximately 2.5 mm either side of center. Testing was linear displacement control with a displacement rate of 0.10 mm/sec using a

Transducer Techniques 5 kg load cell. Fibulas were loaded to failure with data points recorded every 0.01 second. Structural or extrinsic properties, such as ultimate force (Fu; height of curve), stiffness (S; slope of curve), ultimate displacement (du; width of curve), and energy to fracture (U; area under the curve), were calculated from load-displacement curves using Origin® version 7.5 software

Statistical analysis

Two-factor ANOVAs with timepoint (two weeks or four weeks) and genotype (Mstn+/+, +/−, or +/+) as the two factors were run for the histological variables to identify genotype and timepoint effects, as well as possible timepoint*genotype interactions. Single-factor ANOVAs were run among variables collected at each timepoint with genotype as the factor. Post hoc test analysis was done using the Tukey-Kramer Multiple Comparisons test. The unpaired t-test was used to statistically compare biomechanical and gene expression data between myostatin-deficient and normal mice. Statistical comparisons were considered significant at $p < 0.05$.

Results

Two weeks post-surgery

The mice studied two weeks following osteotomy did not differ in body weight (Fig. 1A); however, $Mstn^{-/-}$ mice had significantly larger quadriceps muscles both absolutely (Fig. 1B) and relative to body mass (Fig. 1C). Total callus area is significantly larger in myostatin deficient mice two weeks following surgery (Fig. 1D–F), and osseous tissue area and cartilage area (Cg.Ar) are both elevated in $Mstn^{-/-}$ mice (Fig. 2). Cartilage area relative to callus area (Cg.Ar/C.Ar), and osseous tissue area relative to callus area (TOT.Ar/C.Ar) were similar among groups at this timepoint (Table 2). Two-factor ANOVAs show that, among all the mice, callus size is significantly greater at two weeks than at four weeks (Fig. 2), and that approximately 1/3 of the callus is cartilaginous at two weeks whereas it is almost entirely ossified by four weeks (Table 2). RT-PCR data using either GAPDH or 18s RNA as housekeeping genes showed a significant up-regulation (2.4 fold) of Sox-5 in the myostatin-deficient (−/−) mice (Table 3), and analyses using GAPDH as a housekeeping gene or analyses where the data from GAPDH and 18s RNA were averaged indicate a significant increase in BMP-2 expression (1.5 fold) in the callus of myostatin-deficient (−/−) mice. The data using GAPDH for normalization also show that Runx2 and Osx were down-regulated in the myostatin-deficient animals (Table 3). Two-factor ANOVAs revealed no significant timepoint*genotype interactions for any of the variables.

Four weeks post-surgery

As was the case two weeks following surgery, there was no difference in body weight among the mice at four weeks post-osteotomy (Fig. 3A). $Mstn^{-/-}$ mice do, however, have significantly larger quadriceps muscles than normal mice both absolutely (Fig. 3B) and relative to body mass (Fig. 3C). Histological sections further demonstrate that total callus area is significantly greater in myostatin deficient mice compared to normal mice (Fig. 3D–F); this difference can also be observed from radiographs and microCT images of the ossified callus at four weeks (Fig. 4A, B). Diameter of the callus in myostatin-deficient animals is significantly larger than that of wild-type mice (Fig. 4C, D), even when normalized by diameter of the fibula shaft (Fig. 4D, E). Biomechanical testing experiments demonstrate that the fracture callus of $Mstn^{-/-}$ mice absorbs significantly higher energy to fracture (toughness), yields at a significantly higher peak (ultimate) force, and is also slightly (but not significantly) stiffer than that of normal mice (Fig. 5). Osseous tissue area is significantly greater in myostatin deficient mice four weeks following surgery (Fig. 2), but cartilage area (Cg.Ar), cartilage area relative to callus area (Cg.Ar/C.Ar), and osseous tissue area relative to callus area (TOT.Ar/C.Ar) are similar among groups at this timepoint (Table 2).

Discussion

The morphological and molecular events involved in the process of fracture healing are relatively well understood. The process can be separated into three general phases: an initial inflammatory phase, a chondrogenic phase, and an osteogenic phase [10]. The inflammatory phase is characterized by increased expression of GDF8, BMP2, and Wnt-5A, the chondrogenic phase by elevated expression of GDF5, TGFβ2,3, and beta-catenin, and the osteogenic phase by expression of BMP3,4,7,8, and Frizzled [14]. The role of early GDF8 (myostatin) expression in the callus during the inflammatory phase of fracture healing has, however, been difficult to interpret since this factor is most well known for its effects on myogenesis. It is now known that the receptor for myostatin is expressed in bone-marrow derived stromal cells [8], and that myostatin can stimulate adipogenic differentiation in mesenchymal stem cells whereas its absence increases osteogenic differentiation [8,15]. Myostatin regulates myogenic differentiation in part by suppressing the expression of myogenic factors such as MyoD, but it also inhibits myoblast proliferation by increasing levels of p21 [16]. Results presented here reveal that myostatin deficiency has a significant effect on development of the fracture callus, where mice lacking myostatin show a larger callus at two- and four- weeks post osteotomy. These results suggest that the early expression of myostatin in the callus is likely to suppress the proliferation and recruitment of progenitor cells at the site of injury. It is noteworthy in this regard that the absence of myostatin increases the expression of Sox5, a factor that enhances chondrocyte proliferation and delays chondrocyte maturation and hypertrophy [17], and also decreases the expression of Runx2 and Osx. Likewise, BMP2 is upregulated in the callus of myostatin-deficient mice, and this factor is normally expressed early in fracture healing when it is thought to trigger the subsequent expression of other BMPs later in the healing process [10]. Together these findings indicate that early myostatin expression regulates the initial recruitment and proliferation of progenitor cells in the callus, such that inhibition of GDF8 expression leads to chondrogenic tissue expansion that ultimately increases overall hard callus size and bone volume.

Myostatin and activin both bind the type IIB activin receptor (ActRIIB), and this receptor is highly expressed in proliferating chondrocytes of the healing callus [18]. Immunohistochemical studies by Sakai and colleagues [19] demonstrated that activin is highly expressed in proliferating cells of the fracture callus very early (day two) in the healing process. Activin treatment of the fractured rat fibula yields a phenotype very similar to the one observed in the myostatin-deficient mice examined in this study. Specifically, activin treated animals showed a significant increase in overall callus size, bone volume, and callus strength in three-point bending [19]. Activin itself stimulates osteoblastogenesis in cultured bone marrow stromal cells [20], and activin treatment increases the mass of isografted bone [21]. There are multiple ligands that bind Act RIIB, including activin, myostatin, BMP-7, and BMP-3 [22–26]. Many of these factors antagonize one another. For example, BMP-3 is known to antagonize the osteogenic effects of BMP-7 mediated by ActRIIB [24], and BMP-3 also antagonizes activin signaling [25]. Likewise, myostatin inhibits binding of BMP-7, but not BMP-2, to the type IIB activin receptor [22], and BMP-7 antagonizes activin binding to ActRIIB [26]. It is likely that myostatin expression during the initial phase of fracture healing has anti-osteogenic effects by antagonizing activin and BMP signaling through ActRIIB. We are currently testing this hypothesis using both in vitro and in vivo systems, but the results presented here suggest that inhibition of myostatin signaling early in the healing process may enhance fracture repair by increasing callus size and bone volume. Myostatin inhibitors are well known to improve muscle regeneration [27], and inhibition of the myostatin pathway may therefore promote the integrated regeneration and repair of both muscle and bone in cases of orthopaedic trauma.

Acknowledgements

We are grateful to Kelli Agee and Dr. David Pashley for use of the Vitrodyne, and to Sumont Ponnala (Emory University), Stella Patterson (University of Georgia), and the late Cheryl Mims for assistance with data collection. Funding for this research was provided by the National Institutes of Health (AR 049717) and the Office of Naval Research (N00014-08-1-0197). Two anonymous reviewers provided helpful comments that improved the quality of the manuscript.

References

1. McPherron AC, Lawler AM, Lee S-J. Regulation of skeletal muscle mass in mice by a new TGF-β superfamily member. Nature 1997;387:83–90. [PubMed: 9139826]
2. Schuelke M, Wagner KR, Stolz LE, Hubner C, Riebel T, Komen W, Braun T, Tobin J, Lee SJ. Myostatin mutation associated with gross muscle hypertrophy in a child. New Eng J Med 2004;350:2682–2688. [PubMed: 15215484]
3. Zimmers TA, Davies MV, Koniaris LG, Haynes P, Esquela A, Tomkinson K, McPherron A, Wolfman N, Lee SJ. Induction of cachexia in mice by systemically administered myostatin. Science 2002;296:1486–1488. [PubMed: 12029139]
4. Wagner KR, Liu X, Chang X, Allen RE. Muscle regeneration in the prolonged absence of myostatin. Proc Natl Acad Sci U S A 2005;102:2519–24. [PubMed: 15699335]
5. Hamrick MW. Increased bone mineral density in the femora of GDF8 knockout mice. Anat Rec 2003;272:388–391.
6. Hamrick MW, Pennington C, Byron CD. Bone architecture and disc degeneration in the lumbar spine of mice lacking GDF-8 (myostatin). J Orthop Res 2003;21:1025–1032. [PubMed: 14554215]
7. Nicholson EK, Stock SR, Hamrick MW, Ravosa MJ. Biomineralization and adaptive plasticity of the temporomandibular joint in myostatin knockout mice. Arch Oral Biol 2006;51:37–49. [PubMed: 16054590]
8. Hamrick MW, Shi X, Zhang W, Pennington C, Kang B, Thakore H, Haque M, Isales CM, Fulzele S, Wenger K. Loss of myostatin (GDF8) function increases osteogenic differentiation of bone marrow-derived mesenchymal stem cells but the osteogenic effect is ablated with unloading. Bone 2007;40:1544–1553. [PubMed: 17383950]
9. Bialek P, Parkington J, Warner L, St Andre M, Jian L, Gavin D, Wallace C, Zhang J, Yan G, Root A, Seeherman H, Yaworsky P. Mice treated with a myostatin/GDF-8 decoy receptor, ActRIIB-Fc, exhibit a tremendous increase in bone mass. Bone 2008;42:S46.
10. Cho T, Gerstenfeld L, Einhorn T. Differential temporal expression of members of the transforming growth factor beta superfamily during murine fracture healing. J Bone Miner Res 2002;17:513–520. [PubMed: 11874242]
11. Midura RJ, Ibiwoye MO, Powell KA, Sakai Y, Doehring T, Grabiner M, Patterson T, Zborowski M, Wolfman A. Pulsed electromagnetic field treatments enhance the healing of fibular osteotomies. J Orthop Res 2005;23:1035–1046. [PubMed: 15936919]
12. Hamrick MW, Samaddar T, Pennington C, McCormick J. Increased muscle mass with myostatin deficiency improves gains in bone strength with exercise. J Bone Miner Res 2006;21:477–483. [PubMed: 16491296]
13. Gerstenfeld LC, Wronski TJ, Hollinger JO, Einhorn T. Application of histomorphometric methods to the study of bone repair. J Bone Miner Res 2005;20:1715–1722. [PubMed: 16160729]
14. Hadjiargyrou M, Lombardo F, Zhao S, Ahrens W, Joo J, Ahn H, Jurman M, White D, Rubin C. Transcriptional profiling of bone regeneration. J Biol Chem 2002;277:30177–30182. [PubMed: 12055193]
15. Artaza J, Bhasin S, Magee T, Reisz-Porszasz S, Shen R, Groome N, Fareez M, Gonzalez- Cadavid N. Myostatin inhibits myogenesis and promotes adipogenesis in C3H 10T(1/2) mesenchymal multi-potent cells. Endocrinol 2005;146:3547–57.
16. Lee SJ. Regulation of muscle mass by myostatin. Ann Rev Cell Dev Biol 2004;20:61–86. [PubMed: 15473835]

17. Smits P, Dy P, Mitra S, Lefebvre V. Sox5 and sox 6 are needed to develop and maintain source, columnar, and hypertrophic chondrocytes in the cartilage growth plate. J Cell Biol 2004;164:747–758. [PubMed: 14993235]

18. Nagamine T, Imamura T, Ishidou Y, Kato M, Murata F, Dijke P, Sakou T. Immunohistochemical detection of activin A, follistatin, and activin receptors during fracture healing in the rat. J Orthop Res 1998;16:314–321. [PubMed: 9671926]

19. Sakai R, Miwa K, Eto Y. Local administration of activin promotes fracture healing in the rat fibula fracture model. Bone 1999;25:191–196. [PubMed: 10456384]

20. Gaddy Kurten D, Coker J, Abe E, Jilka R, Manolagas S. Inhibin suppresses and activin stimulates osteoblastogenesis and osteoclastogenesis in murine bone marrow cultures. Endocrinology 2002;143:74–83. [PubMed: 11751595]

21. Hirotani H, Ohtsuka-Isoya M, Mori S, Sakai R, Eto Y, Echigo S, Shinoda H. Activin A increases the mass of grafted bone in C3H/HeJ mice. Calcif Tissue Int 2002;70:330–338. [PubMed: 12004338]

22. Rebbapragada A, Benchabane H, Wrana JL, Celeste A, Attisano L. Myostatin signals through a transforming growth factor beta-like signaling pathway to block adipogenesis. Mol Cell Biol 2003;23:7230–7242. [PubMed: 14517293]

23. Ekaza DJ, Cabello G. The myostatin gene: physiology and pharmacological relevance. Curr Opinion Pharmacol 2002;7:1–6.

24. Bahamonde ME, Lyons KM. BMP3: to be or not to be a BMP. J Bone Jt Surg 2001;83-A(Suppl 1):S56–62.

25. Gamer LW, Nove J, Levin M, Rosen V. BMP-3 is a novel inhibitor of both activin and BMP-4 signaling in Xenopus embryos. Dev Biol 2005;285:156–168. [PubMed: 16054124]

26. Piek E, Afrakhte M, Sampath K, van Zoelen E, Heldin C, Dijke P. Functional antagonism between activin and osteogenic protein-1 in human embryonal carcinoma cells. J Cell Physiol 1999;180:141–149. [PubMed: 10395283]

27. Bogdanovich S, Perkins K, Krag T, Whittemore L, Khurana T. Myostatin-propeptide mediated amelioration of dystrophic pathophysiology. FASEB J 2005;19:543–549. [PubMed: 15791004]

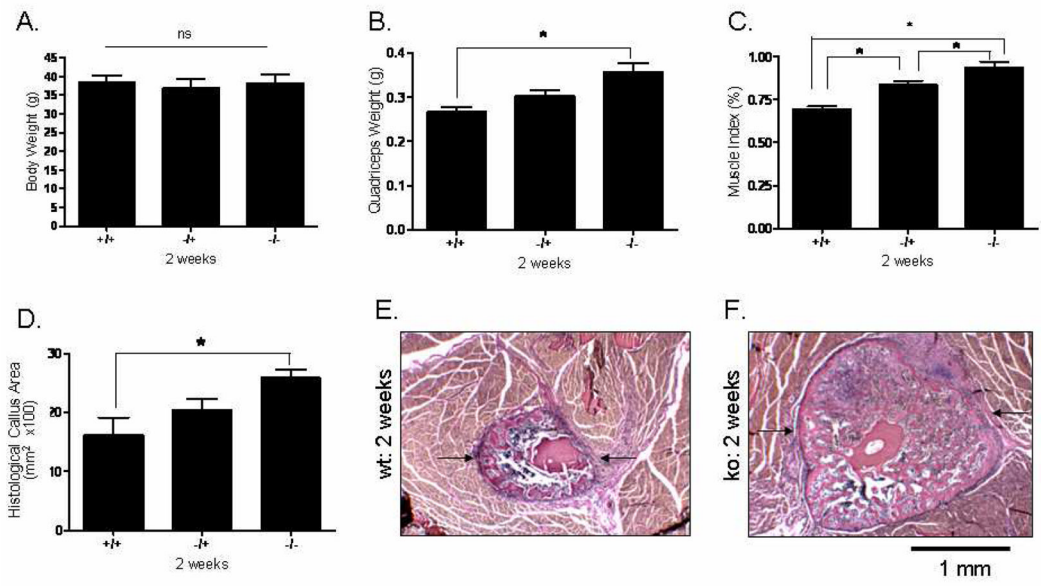

FIG. 1.

Histomorphometric data from the osteotomy site two weeks post-surgery. Top row: Mice do not differ in body weight (Fig. 1A), but $Mstn^{-/-}$ mice have significantly larger quadriceps muscles both absolutely (Fig. 1B) and relative to body mass (Fig. 1C). Bottom row: Total callus area (C.Ar; arrows) is significantly greater in myostatin-deficient mice (Fig. 1D–F). Magnification X40, * $p < 0.05$.

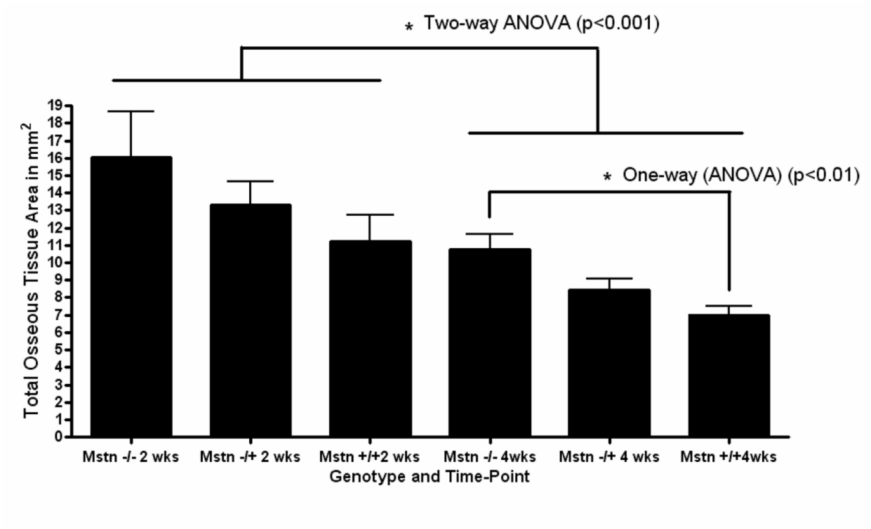

A

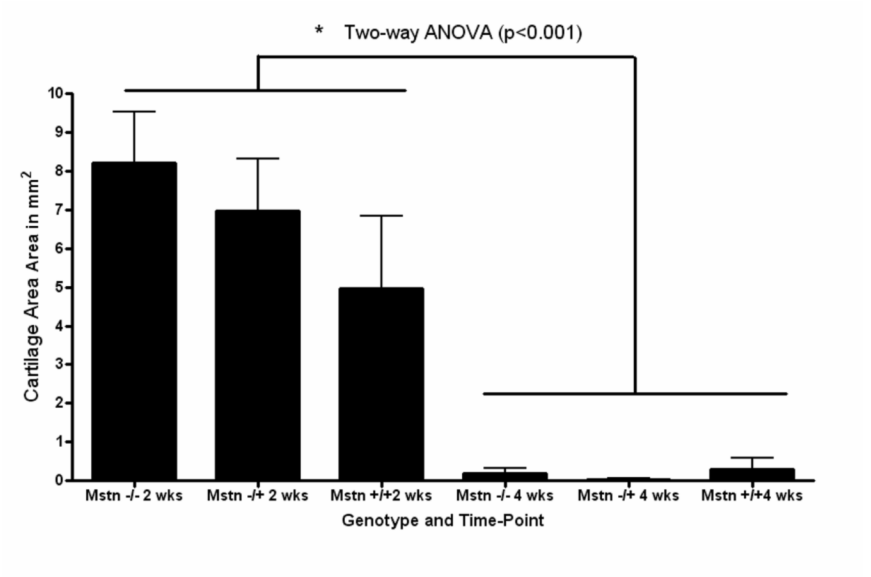

B

FIG. 2.

Total osseous tissue area (A) and total cartilage area (B) of the fracture callus in myostatin-deficient ($Mstn^{-/-}$) mice, mice heterozygous for myostatin ($Mstn^{-/+}$), and normal mice ($Mstn^{+/+}$) at 2 and 4 weeks. Measurments x100, error bars represent 1 S.D.

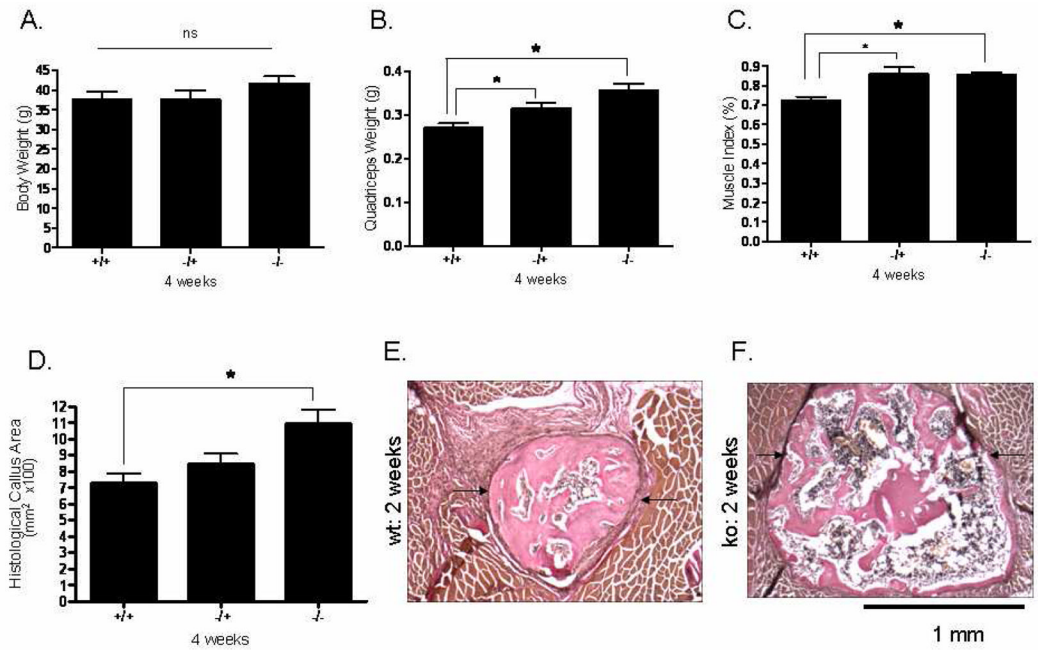

FIG. 3.

Histomorphometric data from the osteotomy site four weeks post-surgery. Top row: There was no difference in body weight among the mice (Fig. 2A), but $Mstn^{-/-}$ and $Mstn^{+/-}$ mice showed significantly greater quadriceps than normal mice both absolutely (Fig. 2B) and relative to body weight (Fig. 2C). Bottom row: Total callus area (C.Ar; arrows) is significantly greater in myostatin deficient mice compared to normal mice (Fig. 2D–F). Magnification X100, * $p < 0.05$.

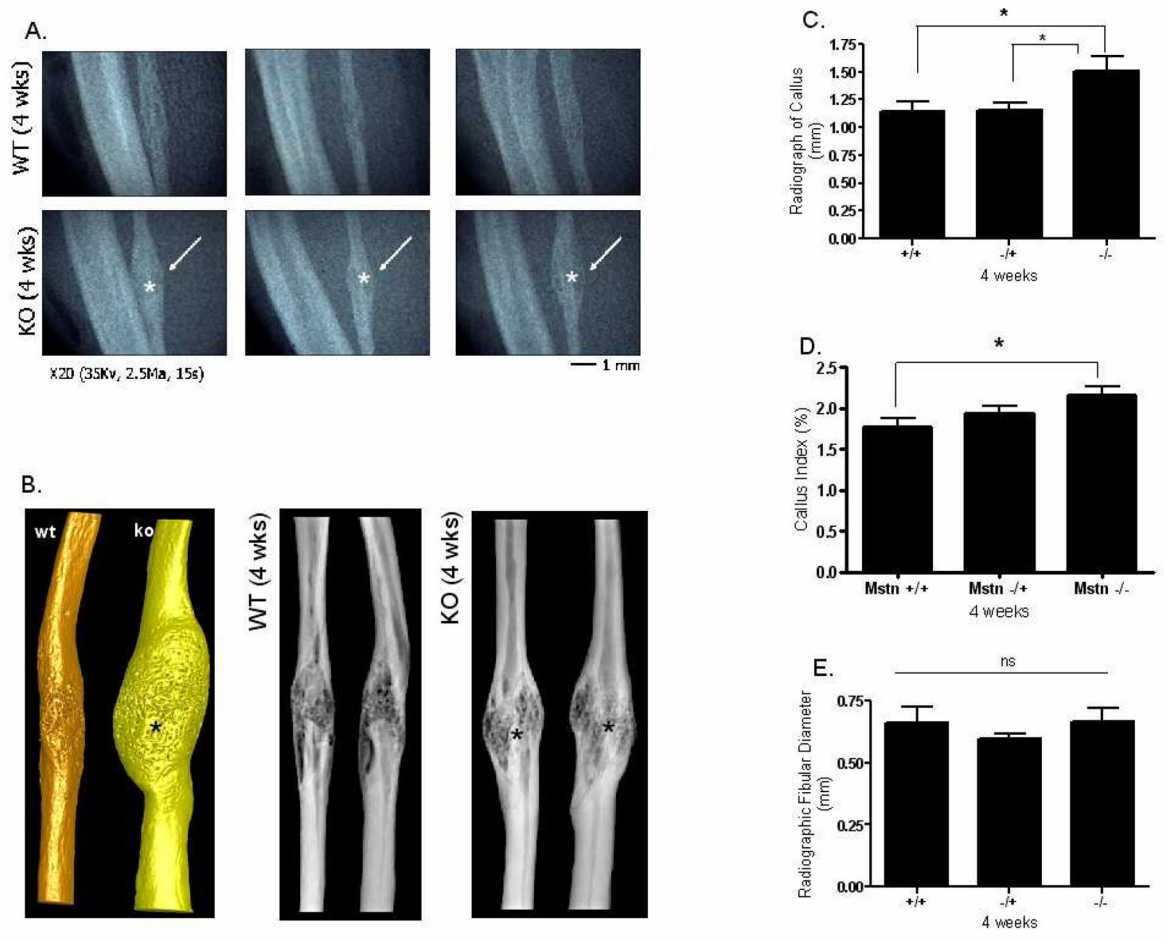

FIG. 4.

Radiographic data from fracture calluses four weeks post-surgery. (A) Faxitron radiographs show that callus size is increased $Mstn^{-/-}$ mice, and (B) microCT images also demonstrate increased bone volume in the fracture callus of $Mstn^{-/-}$ mice. (C) Measurements from radiographs show that $Mstn^{-/-}$ mice have a larger callus diameter, and callus index (D), than normal mice although fibular diameter of the genotypes are similar (E). * $p < 0.05$.

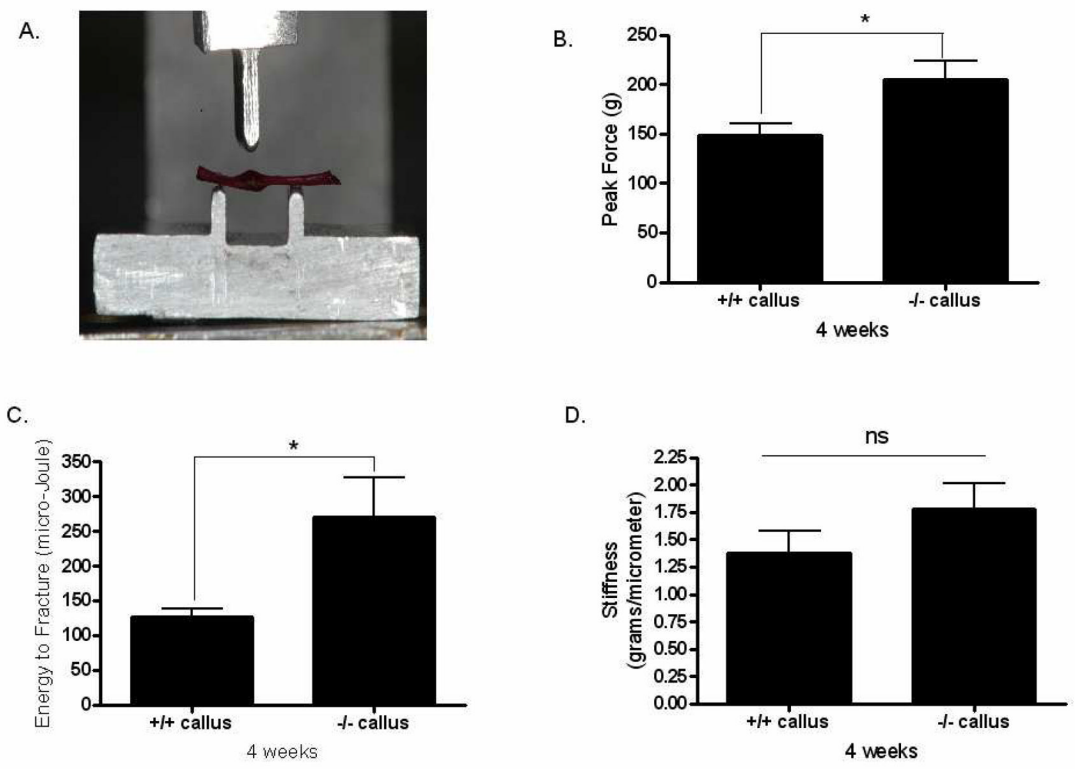

FIG. 5.

Biomechanical data from fracture calluses four weeks post-surgery. (A) Alizarin-red stained fibula specimen showing position of the ossified callus in the three-point bending platform. (B) Ultimate force (peak load) and (C) energy to fracture (toughness) are significantly increased in $Mstn^{-/-}$ mice, and stiffness (D) is non-significantly increased in $Mstn^{-/-}$ mice. * $p < 0.05$.

Table 1

Primer sequences used for analyses of gene expression in the fracture callus two weeks following fibular osteotomy.

Gene	Sequence	Product Size (bp)	Accession Number
Sox-5	F 5′-GTG GAA GAG GAG GAG AGT GAG A -3′	87	BC110478
	R 5′-AAA TTC CTC AGA GTG AGG CTT G -3′		
Sox-9	F 5′-AAA GTT GAT CTG AAG CGA GAG G -3′	123	NM_011448
	R 5′-GAA GGT CTC AAT GTT GGA GAT GA-3′		
Osx	F 5′-ACT ACC CAC CCT TCC CTC AC -3′	101	AY803733
	R 5′-ACT AGG CAG GCA GTC AGA CG -3′		
Col1	F 5′-GCC CAT TAG CCG GTA TGT TAT TA-3′	112	U50767
	R 5′-TCC CTG GTA CCT ATG GAG ACT GT-3′		
BMP-2	F 5′-TGT TTG GCC TGA AGC AGA GA -3′	83	L25602
	R 5′-TGA GTG CCT GCG GTA CAG AT -3′		
18S	F 5′-AGT GCG GGT CAT AAG CTT GC-3′	90	V00851
	R 5′-GGG CCT CAC TAA ACC ATC CA-3′		
GADPH	F 5′-CAT GGC CTC CAA GGA GTA AGA-3′	105	M32599
	R 5′-GAG GGA GAT GCT CAG TGT TGG-3′		
RUNX-2	F 5′-GGA AAG GCA CTG ACT GAC CTA-3′	103	NM_009820
	R 5′-ACA AAT TCT AAG CTT GGG AGG A-3′		

Table 2

Mean (S.D) values for histological parameters of the callus in myostatin-deficient ($Mstn^{-/-}$) mice, mice heterozygous for myostatin ($Mstn^{-/+}$), and normal mice ($Mstn^{+/+}$) at 2 and 4 weeks.

	$Mstn^{-/-}$		**$Mstn^{-/+}$**		**$Mstn^{+/+}$**	
Weeks	two	four	two	four	two	four
Cg.Ar/C.Ar (%) [a]	35.0 (16.0)	1.0 (3.0)	32.0 (16.0)	0.5 (0.5)	30.0 (20.0)	3.0 (9.0)
TOT.Ar/C.Ar (%) [a]	64.0 (16.0)	98.0 (3.0)	67.0 (16.0)	99.0 (0.5)	77.0 (22.0)	97.0 (9.0)

[a] Significant time-point effect, two-factor ANOVA ($p<0.001$)

Table 3

Fold-changes and P-values for comparisons of gene expression in the fracture callus of wild-type (+/+) and myostatin-deficient (−/−) mice two-weeks post-osteotomy using either 18s RNA or GAPDH as housekeeping genes for normalization.

Target sequence	**Fold-change, P-value (t-test)**		
	GAPDH	18s	Combo
Col-I	+0.83, P=0.143	+2.13, P=0.064	+1.77, P=0.124
BMP-2	+0.63, P=0.116	+2.03, P=0.043	+1.55, P=0.055
Runx2	−1.55, P=0.020	−0.03, P=0.940	−2.93, P=0.257
Osx	−1.24, P=0.054	+0.30, P=0.545	−2.37, P=0.377
Sox-5	+1.28, P=0.025	+2.64, P=0.029	+2.43, P=0.022
Sox-9	+0.54, P=0.461	+1.93, P=0.044	+1.45, P=0.144